Selection of Single Scattering from Multiple Scattering Systems by 3D Cross-Correlation. 2. Concentrated Polymer Solutions

L. B. Aberle, M. Kleemeier, and O.-D. Hennemann

Fraunhofer Institute for Manufacturing and Advanced Materials (IFAM), Wiener Str. 12, 28359 Bremen, Germany

W. Burchard*

Institute of Macromolecular Chemistry, University of Freiburg, Stefan Meier Str. 31, 79104 Freiburg, Germany

Received July 11, 2001; Revised Manuscript Received November 9, 2001

ABSTRACT: The effect of multiple scattering from macromolecules was studied on the example of branched amylopectin molecules (waxy maize starch) in water by application of the 3D cross-correlation technique. When the results are compared with those from latex particles of the same hydrodynamic radius, a much weaker influence of multiple scattering on the angular dependence of the static light scattering intensities from amylopectin was observed. Monte Carlo simulations confirmed that this effect can be explained by the weaker decay of the particle scattering factor of the macromolecules compared with hard spheres. Furthermore, we observed no noticeable influence of multiple scattering on the time correlation function (TCF) in dynamic light scattering. We give an attempt of an explanation that is supported by Monte Carlo simulations. Accordingly, the influence decreases with increasing size of the particles or macromolecules. The TCFs of amylopectin were measured at 1% (w/w), 8.7% (w/w), and 20% (w/w). A strong reduction of the segmental mobility was observed as the concentration was increased, and finally hard-sphere behavior was obtained. The observations are in agreement with earlier experimental findings carried out with degraded amylopectins.

Introduction

Static and dynamic light scattering are nowadays well-established techniques in colloid and polymer science. These methods have most successfully been applied to characterizing colloids and polymers in dilute solutions. At sufficiently low concentrations the individual particles or macromolecules are well separated from each other, and their behavior is only little influenced by interparticle interactions. These can fully be eliminated when the data are extrapolated toward zero concentration. The molecular parameters molar mass M_w, radius of gyration $R_g \equiv [\langle S^2 \rangle_z]^{1/2}$, and the shape of the particles, which are obtained for instance from a common Zimm plot, are certainly very relevant parameters, but a close correlation between molecular structure and solid-state properties has yet not been possible.

One way of getting a better understanding of material properties would be to study the polymers or colloids at concentrated solutions and to carry out the extrapolation now toward zero solvent content. Unfortunately, this attractive looking approach proved to be unexpectedly complex. This has two main reasons. The one is the strong influence of the interparticle interactions, and the other is that concentrated solutions mostly become first translucent with a weak bluish shade, then hazy and increasingly turbid with increasing concentration, and finally a white, milky suspension is obtained. Only when almost all solvent is removed from the solution often a clear solid film can be obtained. The high turbidity marked a barrier in the study of such solutions by light scattering. Recently, however, new procedures have been developed by which this barrier could be overcome.

* Corresponding author. E-mail: burchawa@ruf.uni-freiburg.de.

It soon became clear that the high turbidity is correlated to multiple scattering. This is to say, light that is scattered with high intensity by the particles due to the high concentration hits neighbor particles and excite these again to scattering, and this can happen several times. Since the scattered light is emitted in all directions, the light scattered by the other surrounded particles no longer has a defined correlation to the scattering angle of the instrument. All scattering vectors $q = (4\pi n/\lambda_0) \sin(\theta/2)$ in the angular range from $\theta = 0°$ to 180° now contribute and make a structure determination increasingly inaccurate and finally impossible. Here n is the refractive index of the solution, λ_0 the wavelength of the primary beam light, and θ the scattering angle.

This fact has been frustrating mainly in the field of colloid science. With the success in preparing monodisperse latex particles the formation of highly ordered systems at high concentrations became an attractive issue. The interest of polymer scientists in concentrated solutions is more recent. With fascination the formation of supramolecular structures in biological systems is noticed, which fulfill special, highly optimized functions. This structure formation is mostly based on noncovalent bonds and is favored at high concentrations. Scientists are now trying to reveal the principles and to use their knowledge for synthesis of special skeletal structures, artificial muscles, or specific and efficient catalysts. Here again the onset of turbidity prevented the investigation by light scattering.

In the past 20 years it became rather clear how to proceed in order to extract the coherent, singly scattered light intensity from the total scattering intensity that predominantly is determined by multiply scattered light.[1−19] Two different detectors should be used which

10.1021/ma011202y CCC: $22.00
Published on Web 01/29/2002

receive the singly scattered light at the same time and same scattering vector, but on different paths, and the motion of the particles in the same scattering volume should be followed. If only singly scattered light is present, both detectors will measure the same effect. If, on the other hand, a considerable amount of multiple scattering is present, then only the intensity should be selected which detects the same motions on both detectors. This can be done by cross-correlation.

Recently, a fairly simple setup has been developed by one of us that allows selection of the single scattered light component by 3D cross-correlation.[9,12,13,16] Application to concentrated colloidal systems, consisting of polystyrene latices in water, revealed that correct particle scattering factors, and correct hydrodynamic radii are indeed obtained, even for rather turbid suspensions. Neglect of multiple scattering in dynamic light scattering would lead to systematic errors and would wrongly indicate a decrease of the hydrodynamic radii as the concentration was increased. In the present contribution application of the 3D cross-correlation is extended to polymer solutions consisting of the highly branched amylopectin (waxy maize) in water in concentrations up to 20% (w/w). The molecular parameters of this molecularly disperse macromolecule are $M_w = 70 \times 10^6$ g/mol, $R_g = 253$ nm, and $R_h = 316$ nm.[20,21]

Characterization of colloidal and macromolecular systems is complex in concentrated solutions because of the strong interparticle interactions which often lead to pronounced association. In addition, the solutions are often turbid and display pronounced multiple scattering. Macromolecules differ significantly from common colloids by their marked internal or segmental flexibility. For colloids it was sufficient to register only the translational motion of the particles that is described by the mutual diffusion coefficient. In large macromolecules various internal modes of motion superimpose the translational diffusion process and cause a characteristic angular dependence of the apparent diffusion coefficient[22] $D_{app}(q,c) \equiv \Gamma(q,c)/q^2$, where $\Gamma(q,c)$ is the first cumulant in the time correlation function. The segmental mobility is responsible for another difference to colloids. When the concentration of a macromolecule is increased beyond its overlap concentration, flexible chains start to interpenetrate each other.[23] Complete interpenetration is no longer possible with highly branched macromolecules because of the obstacles offered by the many branching points. Therefore, a reduction of the segmental mobility can be expected if the macromolecules are densely pressed together, and this in fact has been observed recently with a cellulose derivative that contained a hard core.[21] It was not evident to us which effect multiple scattering would have on the detection of these internal motions and whether the mentioned observation that was previously made would be an effect of multiple scattering. The choice of a highly branched macromolecule (that in addition has a high tendency to aggregation) for a check of the multiple scattering influence on the time correlation function may appear unnecessarily complicated. However, multiple scattering from noninteracting concentrated *linear* chains is weak and makes such systems not suitable for the mentioned check. Strong multiple scattering arises from heterogeneity caused by large domains of high segment density, which is considerably larger than the average concentration. This requirement is met with waxy maize starch at high concentration.

In the following we will first outline how the field time correlation function can be obtained from measurements of cross-correlation functions. Then results from waxy maize starch at three different concentrations are presented. The actual time correlation functions, the angular dependencies, and the concentration dependence of the various modes of motion are presented. In a next step it will be shown how from measurements of the time cross-correlation functions also the static intensities of singly scattered light are obtained. The angular and concentration dependencies from the starch concentrations are shown. In the discussion a comparison is made between the field TCF obtained from the cross-correlated scattering intensities with the autocorrelation function registered directly from the total scattering intensities. Both the TCF and the static properties are considered. The reasons for the differences to colloidal structures which show no internal mobility are discussed and compared with results from Monte Carlo simulations.

Basic Principles of the 3D Cross-Correlation Technique and the 3D-SLS Method

The normalized 3D cross-correlation function of the scattered light intensity $i(q,t)$ can be written in the form of[9]

$$C(q,t) = \frac{\langle i_A(q,0)\, i_B(q,t)\rangle}{\langle i_A(q)\rangle\langle i_B(q)\rangle} = 1 + R(q)^2 g_1(q,t)^2 \quad (1)$$

where $q = (4\pi n/\lambda_0)\sin(\theta/2)$ is the magnitude of the scattering vector, with n the refractive index of the solution, λ_0 the wavelength of the laser light in a vacuum, and θ the scattering angle. The angular brackets $\langle\cdots\rangle$ represent the time average, which in ergodic systems equals the ensemble average. $i_A(q,t)$ and $i_B(q,t)$ are the intensities of the scattered light detected by two detectors A and B. $\langle i_{A,B}(q)\rangle = \langle i^s_{A,B}(q)\rangle + \langle i^m_{A,B}(q)\rangle$ is the time-averaged intensity of the total scattered light, where the indices s and m denote singly and multiply scattered light, respectively. $g_1(q,t)$ is the normalized correlation function of the electric field of the singly scattered light. Note that the field correlation function $g_1(q,t)$, extracted from cross-correlation measurements, results only from single scattering and therefore is *not* affected by the influence of multiply scattered light. We consider here for the moment only the simplest case. For suspensions containing monodisperse spherical and noninteracting particles $g_1(q,t) = \exp(-\Gamma t)$ with $\Gamma = Dq^2$ where D is the translational diffusion coefficient of the particles. The amplitude $R(q)$ depends strongly on the intensity ratio of the single to the total scattered light but also on the geometric conditions of the experimental setup and on nonoptimized instrumental alignment. It is possible to evaluate the amplitude $R(q)$ quantitatively by carrying out measurements with decreasing concentration c of the scattering particles. In the limit of $c \to 0$ there is no multiple scattering, and the amplitude $R(q)$ of the cross-correlation function $C(q,t)$ reaches its maximum value. Under those conditions the quantity $R(q)$ will be denoted by $R_0(q)$; it is solely determined by geometric parameters of the optical setup and by nonoptimized instrumental alignment. $R_0(q)$ can be used to normalize the amplitude $R(q)$ for an arbitrary sample to obtain $R^*(q) = R(q)/R_0(q)$.

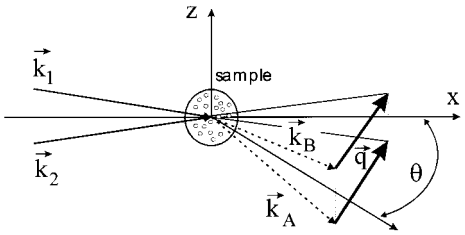

Figure 1. Scattering geometry of the 3D cross-correlation technique.

With this normalized amplitude $R^*(q)$ the single scattered light intensity is[12]

$$\langle i^s(q)\rangle = R^*(q)\langle i(q)\rangle \tag{2}$$

with $\langle i(q)\rangle = \sqrt{\langle i_A(q)\rangle\langle i_B(q)\rangle}$. The intensity ratio of the multiply to the singly scattered light is then given by

$$\frac{\langle i^m(q)\rangle}{\langle i^s(q)\rangle} = \frac{1}{R^*(q)} - 1 \tag{3}$$

We introduce the modified correlation function $g_1^*(q,t) \equiv R^* g_1(q,t)$, which is related to $C(q,t)$ in eq 1 as

$$g_1^*(q,t) = R^* g_1(q,t) = \frac{(C(q,t) - 1)^{1/2}}{R_0(q)} \tag{4}$$

$C(q,t)$ is the measured time cross-correlation function (cross TCF), and the value of $R_0(q)$ is obtained from $C(q,c{=}0) - 1 = R_0^2(q)$, and therefore, $R^*(q) = R(q)/R_0(q)$ and the desired time correlation function of single scattered light $g_1(q,t)$ can experimentally be determined without assumptions.

Experimental Section

Instrumental Setup. The principles of the instrumental construction were already described in previous papers.[9,12,13,16] Here we only repeat some essential features. To fulfill the condition of equal scattering vectors, the vertically polarized beam of a He−Ne laser (35 mW) was split into two beams (in $+z$ and $-z$ directions) by a system (BS) consisting of a beam splitter and a right angle prism mounted on top of the beam splitter (see Figures 1 and 2). The distance between the parallel laser beams was 1 cm. Accurate parallelism of the two laser beams has a sensitive influence on the reliable detection of the cross-correlation function. The tight connection between beam splitter and right angle prism makes this part of the 3D cross-correlation experiment rather insensitive to small perturbations when operating the instrument. This is important because even small misalignment is responded by a reduced cross-correlation signal.

The two laser beams were focused by a lens (L) into the center of a cylindrical thermally controlled cell in which the quadratic sample cell (1 cm × 1 cm) was positioned. To simplify measurements for different scattering angles and to minimize the loss of intensity due to the turbidity and the influence of multiple scattering, the sample cell was positioned such that the distance between scattering volume and cell wall was 0.25 mm.

On the detection side (see Figure 2) the scattered light was collected by two monomode fibers and directed to a matched pair of photomultipliers (ALV/SO-SIPD, Langen, Germany) working in the pulse counting mode. The incoming beams and the two monomode fibers were aligned in such a way as to collect the components of the scattered light to the same scattering vector. Optimized alignment was obtained by a small mirror positioned in the light path leading from the scattering center to one of the two detectors. Finally, the signals of the photomultipliers were processed by a digital correlator (ALV-5000).

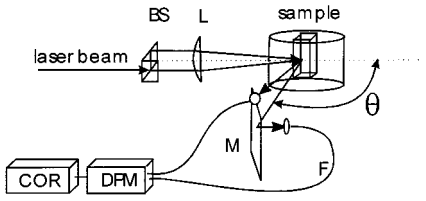

Figure 2. Experimental setup of the 3D principle. A description is given in the text.

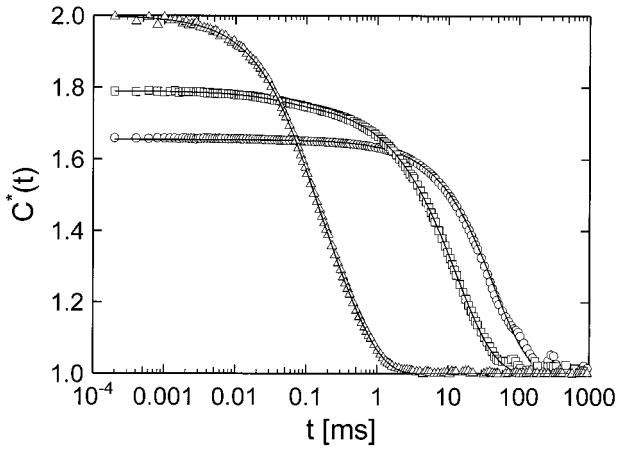

Figure 3. 3D cross-correlation functions for differently concentrated solutions of waxy maize at an scattering angle of $\theta = 90°$: 1% (△), 8.7% (□), 20% (○).

Measurements. Waxy maize starch (amylopectin): We investigated polymer solutions consisting of the highly branched, water-soluble amylopectin (waxy maize) in concentrations of 1.0%, 8.7%, and 20% (w/w). The solutions required a special pretreatment because starches are commonly supplied in their native granule forms which consist of a semicrystalline supramolecular structure.[25,26] The crystalline structure was fully broken up by autoclaving a concentrated aqueous suspension (approximately 15% (w/v)) at 150 °C for 20 min, where a laboratory autoclave "BEP Buechiglasuster" of 250 mL (Buechi AG, Uster Switzerland) was used. To remove dissolved air from the water, argon gas was led through the suspension for a few minutes before the autoclave was tightly closed and kept under the argon atmosphere at 8 bar. The milky suspension became clear at the elevated temperature. After cooling to about 80 °C the autoclave was opened, and the solution was then filtered through a common laboratory paper filter set to remove nonstarch insoluble byproducts. The solution was freeze-dried, and the powder was kept in closed glasses until use.

Starches have a large tendency to aggregation,[20,27] and this required a second heating step of the solution to about 120 °C immediately before use. On cooling the solution to room temperature, the fairly clear solution became again slightly turbid. The turbidity τ_t for the differently concentrated samples was determined by measurements of the transmitted intensity of the laser beam as usual. We obtained $\tau_t = 0.0$, 0.63, and 1.72 cm^{-1}, respectively, for the mentioned concentrations. The 1% concentration was filtered through a hydrophilic filter of 5 μm in pore size (Sartorius, Goettingen, Germany). The higher concentrations no longer could be filtered and were used without further pretreatment.

Results

Dynamic Light Scattering. Figure 3 shows the correlation functions $C^*(q,t) = 1 + R^{*2} g_1(t)^2$ obtained by 3D cross-correlation for three different concentrations. In this case the scattering angle was fixed at 90°. The amplitude $R^*(q)$ of the cross-correlation function $C^*(q,t) - 1$ from the 1% solution was close to the value

Table 1. Angular Dependencies of the Scaling Exponents n_s and n_f for Different Temperatures in the Range 20−50 °C

	c (w/w) = 20.0%	c (w/w) = 8.7%		c (w/w) = 1.0%	
T [°C]	n_s	n_s	n_f	n_s	n_f
50	1.82 ± 0.12	1.35 ± 0.1	1.63 ± 0.11	2.61 ± 0.07	2.14 ± 0.07
40	2.17 ± 0.06	2.02 ± 0.15	0.95 ± 0.22	2.52 ± 0.03	2.07 ± 0.03
30	1.98 ± 0.05	2.34 ± 0.11	0.83 ± 0.12	2.44 ± 0.05	2.07 ± 0.05
20	2.04 ± 0.21	1.59 ± 0.17	0.81 ± 0.44	2.29 ± 0.03	1.95 ± 0.04

of 1 as expected for single scattered light. However, the value of $R^*(q)$ decreased strongly with increasing concentration of the polymer solution. This indicated the increasing influence of multiple scattering. According to eq 2, the amplitude $R^*(q)$ equals the ratio of single to total scattered light and therefore directly yields a quantitative measure to which extent multiple scattering influences the detected intensity of the total scattered light.

In dilute solution the time correlation function (TCF) mostly shows only one relaxation process. In concentrated solution this mode becomes somewhat faster, and in addition, a second slow relaxation process occurs. The measured TCFs were fitted by the well-known Kohlrausch−Williams−Watts[28] (KWW) approach with one stretched and one single-exponential according to the equation

$$g_1(q,t) = A_s \exp[-(t/\tau_s)^{\beta}] + A_f \exp(-\Gamma_f t) \qquad (5)$$

where the subscripts s and f indicate slow and fast mode of motions. τ_s denotes a relaxation time, and its mean value is given by

$$\langle\tau_s\rangle = (\tau_s/\beta)\Gamma(1/\beta) \qquad (6)$$

$\Gamma(x)$ is the common gamma function and has to be distinguished from the decay constants Γ_s or Γ_f of the correlation functions. These decay constants are usually obtained from cumulant fits based on the equation

$$-\ln g_1(q,t) = \Gamma t + \Gamma_2 t^2 + \Gamma_3 t^3 + \ldots \qquad (7)$$

The decay constant Γ (first cumulant) in a good approximation is

$$\Gamma \approx 1/\langle\tau\rangle \qquad (8)$$

if β is larger than 0.5. The exponent β is a measure of the width for the relaxation distribution. For the slow mode it exhibited only a slight angular dependence and, within experimental errors, no detectable concentration dependence. The value of $\beta = 0.86 \pm 0.05$ is typical for a polydisperse system which shows only little or no internal segmental mobility. The fast mode was difficult to register accurately. Therefore, the indicated single-exponential behavior (second term in eq 6) was assumed.

Figure 4 shows the contribution A_f of the fast mode in the system as a function of the scattering angle θ for the two concentrations $c = 1\%$ (w/w, filled symbols) and $c = 8.7\%$ (w/w, open symbols). As expected, the influence of the fast motion decreases drastically for the high concentration. Both concentrations show significant angular dependence. For the 20% solution the fast mode amplitude was already below the detection limit, and the slow motion was fully dominant. Only for the 1% solution the contribution of the fast motion increased with temperature, but the change from 0.17 to 0.23 still remained small.

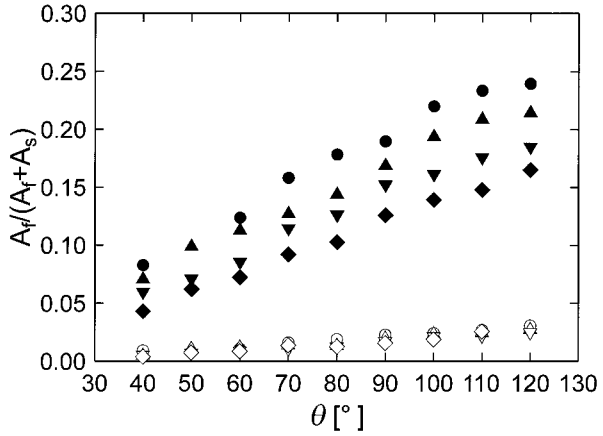

Figure 4. Contribution of the fast mode for the 8.7% (open symbols) and 1% (filled symbols) solutions. The measurements were performed at 50 (●, ○), 40 (▲, △), 30 (▼, ▽), and 20 °C (◆, ◇).

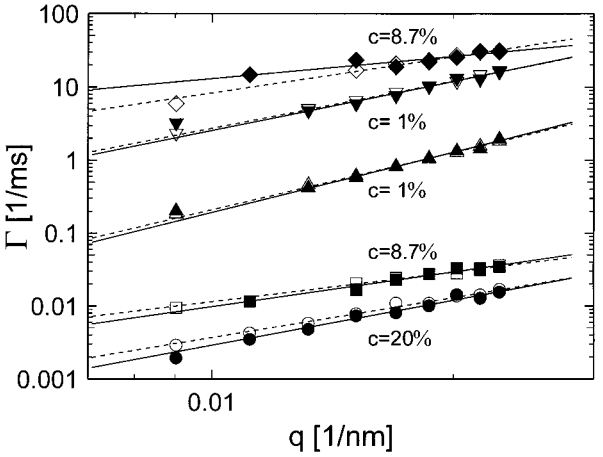

Figure 5. Angular dependence of the decay constants Γ_s and Γ_f for the different concentrated waxy maize solutions: open and full symbols represent the results obtained from auto- and cross-correlation function, respectively. The measurements were performed at 50 °C.

Both decay constants $\Gamma_s = 1/\langle\tau_s\rangle$ and $\Gamma_f = 1/\langle\tau_f\rangle$ are usually angular and concentration dependent. The angular dependencies are shown in Figure 5 in a double-logarithmic plot of Γ_s and Γ_f against q for a temperature of $T = 50$ °C. The angular dependence of the decay constants can be expressed by a the scaling law $\Gamma \sim q^n$. The exponents n_s and n_f for the slow and fast decay are given in Table 1.

Most values of the scaling exponents in the angular dependence are around the value 2, which is expected for diffusive motions. Interestingly, the exponent for the slow motion in the 1% solution is larger than 2. Such behavior is expected for large particles with internal modes of motion under the influence of hydrodynamic interactions (Zimm-type relaxation modes[29,30]). Theory predicts an asymptotic limit of $n_s = 3$, which apparently was not yet reached in our experiment. Note, for the Rouse limit (no hydrodynamic interaction) the limiting

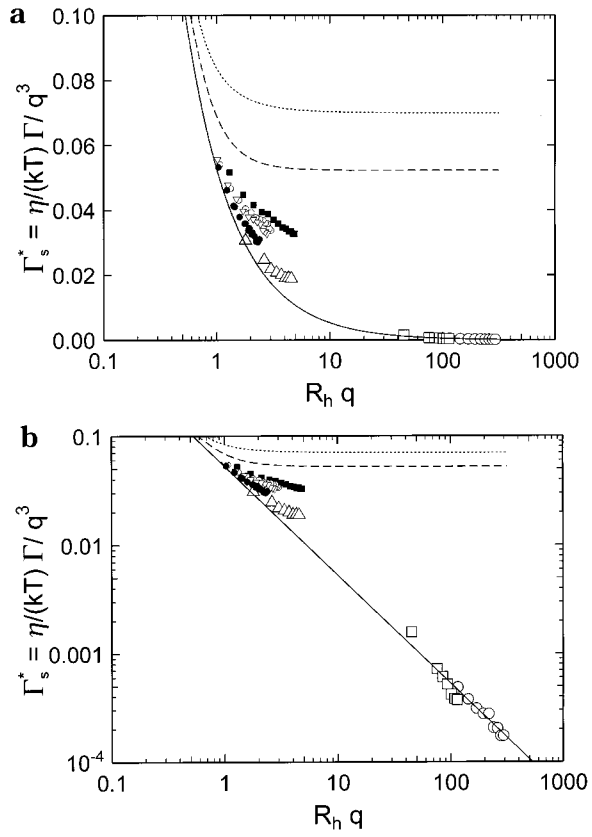

Figure 6. Master plot for the decay constant Γ_s of the slow mode: Values for $\Gamma^* = (\Gamma/q^3)\eta/(kT)$ vs $R_h q$. (a) Linear−log plot, (b) log−log plot. The large symbols (○: c = 20%; □: c = 8.7%; △: c = 1%) represent the values obtained in this paper; the small symbols are data taken from a previous paper.[31] The concentration increases in the order (■, ○, ▽, ●). Hard-sphere behavior is given by the solid line; the dotted and dashed lines represent results expected for flexible chains in good and Θ solvents, respectively.

value is even $n_s = 4$. The low values for the fast mode exponent n_f in the 8.7% solution cannot be explained by theory. However, the influence of the fast motion at this concentration is already so small that no reliable determination of the exponent seems to be possible.

Another way of checking the angular dependencies is a plot of[29]

$$\Gamma^* = (\eta/kT)(\Gamma/q^3) \tag{9}$$

against qR_h, where R_h is the effective hydrodynamic radius derived from the Stokes−Einstein relationship

$$R_h = (RT/6\pi\eta)(q^2/\Gamma)|_{\text{at } q=0} \tag{10}$$

The data for the slow motion are presented in Figure 6a in a plot of Γ_s^* against $\log(qR_h)$, where for comparison data from other degraded starches are added.[31,32] For the two high concentrations the values for Γ_s^* are close to zero, and differences between the two concentrations are hardly noticeable. This is better recognized in Figure 6b where the same data of Figure 6a were now plotted in a double-logarithmic scale. The full line corresponds to $\Gamma_s^* = 1/(6\pi qR_h)$, which is characteristic of hard-sphere behavior (no internal motions). The data from the two highest concentrations follow this line, but for the 1% solution, which is still about 3 times the overlap

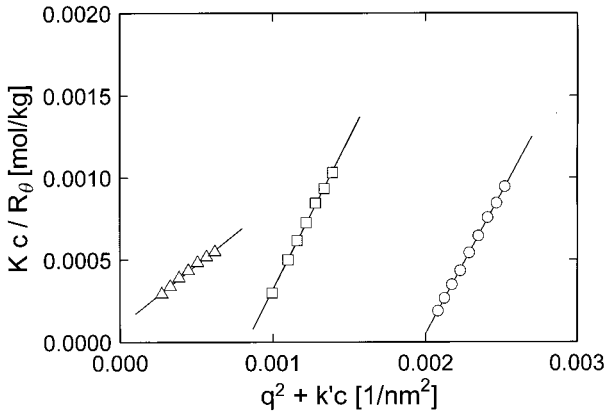

Figure 7. Zimm plot for the different concentrated waxy maize starch solutions 1% (△), 8.7% (□), and 20% (○) at 50 °C.

concentration, the data show systematic deviations at high qR_h. For the concentration dependence see the discussion.

Static Light Scattering. Originally the purpose of cross-correlation spectroscopy was to investigate dynamic properties of samples in turbid systems. On a conference in 1997 and in the subsequent paper one of us[8,9] demonstrated that in addition also the corresponding coherent static scattered light can be obtained, which gives valuable information on the equilibrium structure of the polymers in concentrated systems. In the following this was confirmed by several other authors.[10,15,19] The key relationship is given by eq 2. The single scattered light intensity $\langle i^s(q)\rangle$ can be obtained from the cross-correlation experiments without introducing assumptions because $\langle i(q)\rangle$ and $R^*(q)$ are experimentally accessible quantities. The intensity of the singly scattered light $\langle i^s(q)\rangle$ has to be corrected for the turbidity. The Rayleigh ratio R_θ is then derived as follows:

$$R_\theta = \langle i^s(q)\rangle \exp(\tau_t l)(R_{\text{toluene}}/\langle i_{\text{toluene}}\rangle)/V_{sc}(\theta) \tag{11}$$

In this relationship τ_t denotes the turbidity of the solution and l the path length of the light in the medium. $V_{sc}(\theta)$ represents a correction for the scattering volume. In conventional light scattering experiments $V_{sc}(\theta) = 1/\sin(\theta)$, but for the 3D cross-correlation setup the situation is somewhat more complex because of the two crossing laser beams. Here, $V_{sc}(\theta)$ can be described by the empirical equation $V_{sc}(\theta)/V_{sc}(\theta{=}90°) = (1 - B) + B/\sin(\theta)$ with a constant $B = 0.84 \pm 0.02$, which was obtained by measuring samples with isotropic scattering characteristics. The Rayleigh ratio for toluene was taken from the literature.[33,34] The value for the HeNe laser light at $\lambda_0 = 632.8$ nm is $R_{\text{toluene}} = 12.46 \times 10^{-6}$ cm^{-1}.

Figure 7 shows the result of the scattering intensities $\langle i^s(q)\rangle$ from the three concentrations in form of a common Zimm plot where Kc/R_θ is plotted against $q^2 + k'c$, where K is the optical contrast factor and k' is an arbitrary constant which causes a shift of the curves from the different concentrations proportional to the applied concentration. From the initial slopes of each q^2 curve an apparent mean-square radius of gyration $R^2_{g,app} = 3$ (initial slope/intercept) is obtained; the intercept gives the reciprocal apparent molar mass $1/M_{app}(c)$ of the particles. Both quantities, the radius of gyration and the molar mass, are apparent values, because in semidilute solution these data are strongly affected by interparticle interactions. However, even after correc-

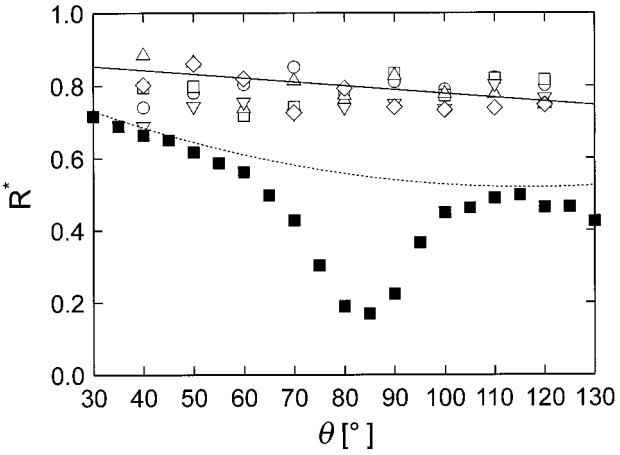

Figure 8. Intensity ratio $\langle I^s(\theta)\rangle/\langle I(\theta)\rangle$ of singly to total scattered light. The turbidity of the investigated samples was $\tau = 1.72$ cm^{-1} for different temperatures: 50 (□), 45 (○), 40 (△), 30 (▽), and 20 °C (◇). The solid and dotted lines are calculated by Monte Carlo simulation. The solid line gives the results expected for the scattering setup used in this work, while the dotted line shows the result that would be obtained for a round sample cell with inner diameter of 1 cm. For comparison, the figure also shows $\langle I^s(\theta)\rangle/\langle I(\theta)\rangle$ obtained experimentally from standard latex particles with $R_g = 175{,}5$ nm (◇), the distance between scattering volume and cell wall was 0.5 mm, and the turbidity was 2.12 cm^{-1}.

tion for this interaction, the molar mass would not coincide with that at infinite dilution because of the formation of aggregates due to hydrogen bonding between the many OH groups of the starch.[20,35] The scattering curves for all concentrations follow nicely, over the whole q range, the prediction of the Ornstein−Zernike approach

$$R_\theta \sim 1/(1 + \xi^2 q^2) \tag{12}$$

The correlation length ξ used in the Ornstein−Zernike approach is uniquely related to the apparent radius of gyration by the relationship

$$\xi = (1/3)^{1/2} R_{g,app} \tag{13}$$

Besides the expected concentration dependence, the apparent radii of gyration also show a certain temperature dependence, which will be discussed later in this paper.

A sensitive test for the validity of the Ornstein−Zernike approach is obtained by a Kratky plot, i.e., a plot of $u^2P(u)$ against u, where $u = qR_g$ and $P(u) = R_\theta/R_{\theta=0}$. In Figure 11 the full line corresponds to the Ornstein−Zernike approach, and the dashed line represents the Kratky plot for amylopectin in *dilute* solution.[20] The Ornstein−Zernike equation holds for polydisperse linear chains but also for randomly branched aggregated macromolecules. The dashed line gives the theoretical prediction for hyperbranched individual macromolecules.

Discussion

Static Light Scattering. First, the influence of multiply scattered light in static light scattering may be considered. The amplitude $R^*(\theta)$ of the measured 3D cross-correlation functions gives the intensity ratio of single to total scattered light $R^*(\theta) = \langle I^s(\theta)\rangle/\langle I(\theta)\rangle$. The results for $R^*(\theta)$ for the turbid sample of $c = 20\%$ are shown in Figure 8 (open symbols). Within the limits of experimental error no angular dependence of $\langle I^s(\theta)\rangle/\langle I(\theta)\rangle$ was observed. The fraction of single scattered light was for all scattering angles about 80%; i.e., for our experimental setup the intensity of multiple scattered light had a similar angle dependence as the single scattered

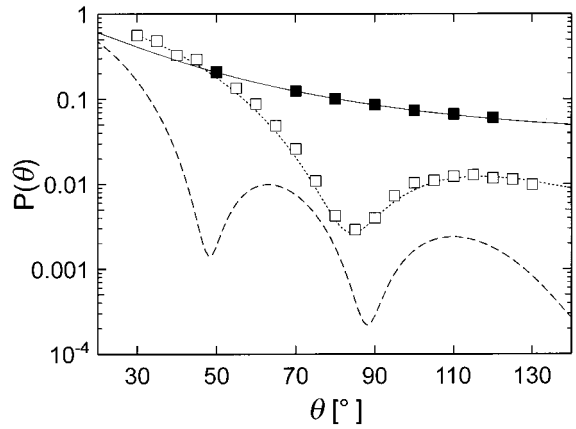

Figure 9. Singly scattered light intensity of the amylopectin solution (■) with concentration 8.7% and $R_g = 300$ nm. The solid line represents the result from the Ornstein−Zernike calculation. For comparison, the symbols □ show the scattering form factor of polystyrene particles with $R_g = 175.5$ nm. The dotted line represents calculation on the basis of the Mie theory. The broken line represents Mie calculations for a hard sphere and $R_g = 300$ nm.

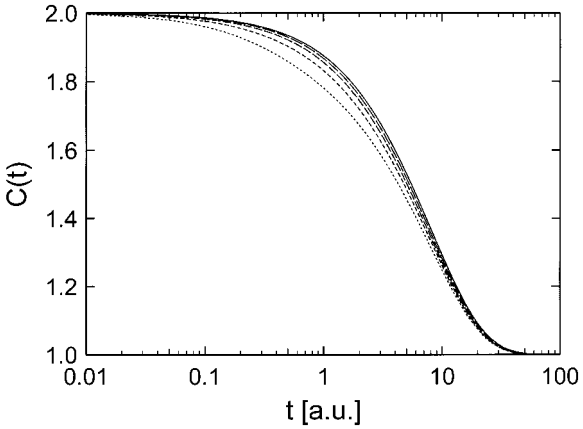

Figure 10. Autocorrelation functions calculated a Monte Carlo simulation. For a description see text.

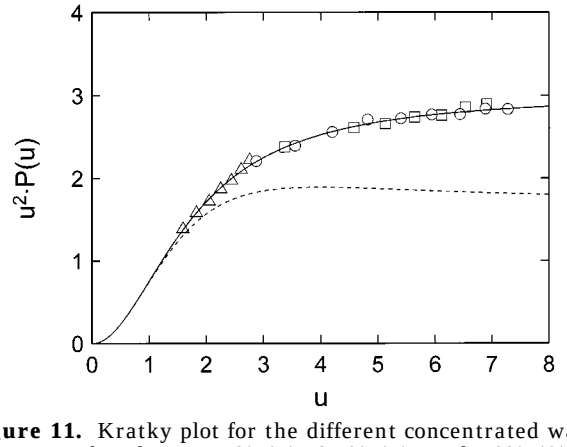

Figure 11. Kratky plot for the different concentrated waxy maize starch solutions 1% (△), 8.7% (□), and 20% (○) at 50 °C. The full line represents behavior according to the Ornstein−Zernike density correlation function; the angular dependence of the dashed line was obtained with the waxy maize starch in the limit of infinite dilution.[20,21]

light. This result was not expected, because standard latex particles of similar R_g showed under similar conditions a much stronger angular dependence of $R^*(\theta)$.[9] Figure 8 shows for example the results of $R^*(q)$ for a standard latex of 453 nm in diameter ($R_g = 175.5$ nm) and turbidity $\tau_t = 2.12$ cm^{-1} (filled symbols). An explanation of this effect is seen in the fact that for the same R_g the amylopectin shows a different angular dependence of the *single* scattered light than the corresponding colloidal latex particles (see Figure 9). For latex particles the scattering dissymmetry at scattering angles $\theta = 30°$ and $\theta = 130°$ is $\langle i_{30}\rangle/\langle i_{130}\rangle \sim 100$; for amylopectin, however, its value is only $\langle i_{30}\rangle/\langle i_{130}\rangle \sim 3$. Therefore, also the *multiply* scattered light of the amylopectin solution shows a much weaker angular dependence than of the latex particle suspension. This leads to an even weaker angular dependence for $R^*(q)$. In contrast to amylopectin, the differential scattering cross section of the latex particles with $R_g = 175$ nm has a strong scattering in forward directions and a rather low one at large angles. The influence of *multiply* scattered light on its angular dependence is stronger for scattering angles where the intensity of *singly* scattered light is low, and $R^*(q)$ decreases with increasing θ.

Monte Carlo Simulations. To check the result for the waxy maize sample, we also performed Monte Carlo simulations on the basis of the procedure presented by Bailey and Cannell.[36] The procedure was outlined in detail in a previous paper[12] and was tested on the basis of the experimental results from the 3D cross-correlation technique. In short, the Monte Carlo method models the incident laser beam by a large number of "photons" which are launched into the sample. In the simulation process the free path length is defined by the distance a photon travels between two scattering processes. The probability distribution of these distances is connected to the turbidity of the scattering medium. The free path length of a photon, counted from the position where it enters the sample to the first scattering process, is chosen at random. If, after traveling this distance, the photon is still located within the sample, it is scattered. The probability for a certain scattering direction is given by the angular dependence of the particle scattering cross section. After that event the photon travels again along a randomly chosen free path length and is possibly scattered anew. If the last scattering event of the photon, before leaving the sample, is within a predefined volume, the scattering event is recorded, where the predefined volume is given by the geometry of the detection optics. In that way the numbers of single, double, and multiple scattered photons for various scattering angles become available and can be compared with the experiment.

The simulations (solid line in Figure 8) confirmed the amylopectin experimental findings (open symbols) for the intensity ratio of single to total scattered light. A slight angular dependence was predicted for $\langle I^s(\theta)\rangle/\langle I(\theta)\rangle$ by the simulations, which was too small to be observed experimentally.

Experiments and simulations were carried out for an optical path with the scattering volume that was placed 0.25 mm apart from the wall of the square scattering cell. If the scattering volume is placed in the *center* of a cylindrical cell, the multiple scattering increases markedly because of the increase of the optical path length in the scattering cell. To receive an impression on the effect, we also carried out Monte Carlo simulations for a round cell of 10 mm in diameter. The result of both Monte Carlo simulations are compared in Figure 8 (solid and broken lines, respectively). Now a significant angular dependence of $R^* = \langle I^s(\theta)\rangle/\langle I(\theta)\rangle$ is predicted with a much stronger decrease at large scattering angles.

Dynamic Light Scattering. Next, the question is examined whether the multiple scattered light has an effect on the time correlation functions. For this purpose we compare the cross-correlation functions $g_1^{cross}(t)$, which in principle are not influenced by multiple scattering, with autocorrelation functions $g_1^{auto}(t)$, where such an influence may be present, at least for turbid samples. Our setup permitted simultaneous registration of the auto- and cross-correlation functions $g_1^{auto}(t)$ and $g_1^{cross}(t)$, respectively. Figure 5 shows decay constants Γ_s and Γ_f for the slow and fast modes as obtained from autocorrelation and 3D cross-correlation functions for e.g. $T = 50$ °C. As expected, no difference in the results for the 1% solution was observed. Also, for the higher concentrated and considerably turbid samples there is no distinguishable difference. Both auto- and cross-correlation functions yield the same decay constants for the concentrated waxy maize solutions.

At a first sight, this result was surprising for us, at least for the 20% waxy maize solution, which was rather turbid. However, the influence of multiple scattering becomes less important as the particles grow in size. This was demonstrated by Monte Carlo simulations with particles of increasing size obeying Ornstein−Zernike scattering characteristics. The simulated intensity correlation function $C^*(t)$ is shown in Figure 10 for a turbidity of $\tau = 2.0$ cm^{-1}, a scattering angle of $\theta = 20°$, and particles with radii of gyration $R_g = 27$, 58, 127, and 266 nm (dashed lines). The solid line represents the TCF which would be obtained in the absence of multiple scattering. Note that for all particles the diffusion constant has been artificially fixed to the same value, so that the change in the curve forms with decreasing particle diameter becomes clearer.

The effect of large sizes on the TCF in turbid systems can be understood as follows. In a multiple scattering process the scattered intensity at a chosen q value results from many other q vectors. At small scattering angles θ the probability of scattering vectors larger than the experimentally chosen one q_{exp} is high and results in an average, which contains also the effects from large scattering angles. This leads to a faster relaxation and thus a larger decay value of Γ. On the other hand, at large scattering angles, both larger and smaller intermediate scattering vectors contribute and cause partial canceling of their influence. With increasing particle size the scattering functions decrease more sharply with q, and the multiple scattering loses influence in the angular range of the instrument. This consideration qualitatively explains why the influence of multiple scattering decreases with increasing particle size but remains pronounced for forward scattering, i.e., at $\theta = 0°$. As a result, we find a filtering-off of the multiple scattered light with increasing particle size, imposing less influence on the dynamic light scattering.

Concentration and Temperature Dependence. The properties of the aqueous dilute solution of waxy maize have been published previously.[20,21] The interpretation of the data offered no difficulties since no turbidity was observed. New effects occurred when the overlap concentration c^* was exceeded. This is a

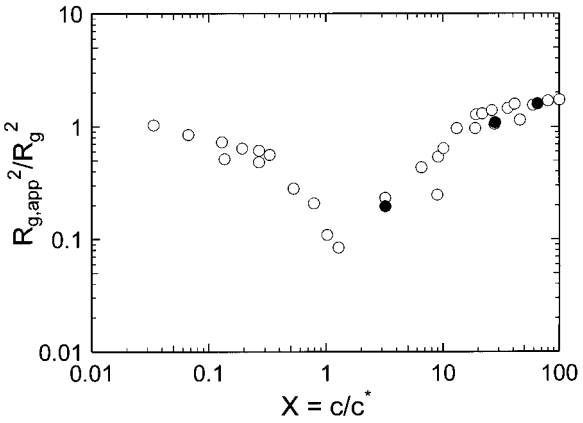

Figure 12. Plot of the apparent to the true mean-square radii of gyration as a function of the reduced concentration $X = c/c^*$: open circles, ref 23; filled symbols, this work.

Table 2. Concentration-Dependent Apparent Molar Masses $M_{w,app}(c)$, Radii of Gyration $R_{g,app}(c)$, and Hydrodynamic Radii $R_h(c)$ for a Temperature of $T = 50$ °C

c (w/w)/%	$M_{w,app}(c)/(10^6$ g/mol)	$R_{g,app}(c)$/nm	$R_h(c)$/nm
1	5.86	112	200
8.7	12.6	264	5000
20	19.6	320	13000

concentration where the molecules start to overlap, but in contrast to flexible linear chains only partial interpenetration can occur with these branched macromolecules as the branching points prevent deep interpenetration. The overlap concentration $c^* = (A_2M_w)^{-1}$ was found to be $c^* = 0.3\%$ (w/v). In this equation A_2 is the second virial coefficient and M_w the weight-averaged molar mass of the amylopectin that had to be determined at zero concentration. In the present case the concentration of the investigated solutions was about 3−66 times higher than c^*. In this concentration regime the properties of individual molecules no longer can be determined, but all measured quantities are strongly influenced by interparticle interactions. Therefore, only apparent molar masses and radii can be obtained. The problem becomes even more involved due to the strong tendency of amylopectin molecules to association. Unfortunately, no equilibrium is obtained, and as a result a more or less pronounced time dependence can occur. This fact has to be kept in mind when the following results are considered.

Table 2 gives a list of the apparent molar masses M_w, radii of gyration R_g, and the effective hydrodynamic radii R_h. As expected from the discussion in the previous sections, neither R_g nor R_h is noticeably affected by multiple scattering in this special example. We wish to emphasize that this result should not be generalized. For instance, for the latex particles measured previously differences have been well observed[9,12,16] even when the scattering volume is positioned near the cell wall. Far more pronounced effects due to multiple scattering are observed when the scattering volume is positioned in the center of the cell, and this holds also for the amylopectin solution.

In this connection it is of interest to compare the present results for the radii of gyration with those measured previously[23] (see Figure 12). Within experimental error of ±10% complete agreement is observed.

The apparent molar masses $M_{w,app}(c)$, however, are affected by multiple scattering. In the case of amylopectin the effect was not larger than 20% (see Figure 8). This very small effect is in particular due to the fact that the scattering volume was positioned very close to the cell wall. For the latex particles in Figure 8 this effect was more pronounced, as a result of slightly higher turbidity ($\tau_t = 2.1$ cm^{-1}), a somewhat larger distance of the scattering volume (0.5 mm) to the cell wall but mainly due to much stronger forward scattering of the hard spheres.

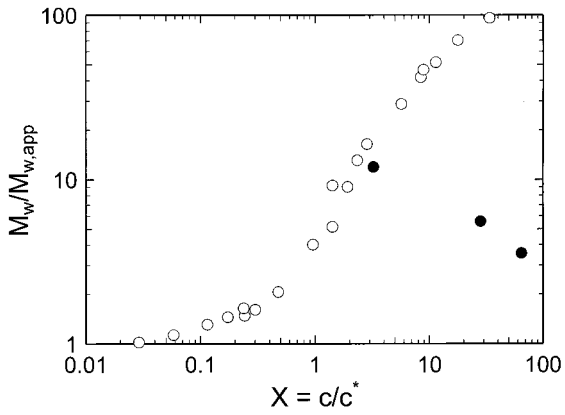

Figure 13. Plot of the ratio of the true to the apparent molar mass as a function of reduced concentration $X = c/c^*$: open circles, ref 23; filled symbols, this work.

Unfortunately, the present results of the apparent molar masses $M_{w,app}(c)$ cannot instructively be compared. The result is shown in Figure 13 which shows an even higher molar mass for the single scattered light than for the total scattered light after correction for turbidity. This is opposite to the expected effect of multiple scattering. The reason for this discrepancy was already mentioned above and is an effect of our incomplete dissolution when heating the samples only to 120 °C instead to 150 °C as was done in the previous work.[23] Because of this incomplete dissolution also the association proceeded faster in time than published before. In fact, the autoclaved solution at 150 °C showed only a weak turbidity and slow aging. It is tempting to compare the molar mass dependent radius R_g of the present apparent data with those obtained in dilute solution. However, one has to keep in mind that the apparent data are strongly affected by interparticle interactions and are thus not really comparable with the true molecular parameters at infinite dilution.

Change of the Angular Dependence in Dynamic Light Scattering with Concentration. In Figure 6a,b the different experimental curves for Γ^* vs R_h q are shown, and the present data were compared with those obtained by Galinsky and Burchard,[31] who measured the concentration dependence for a degraded starch. In both cases the curves approach more and more hard-sphere behavior when concentration is increased. For the flexible linear chains the curves approach a rather high constant plateau. On the other hand, the hard sphere possesses no internal segmental mobility. Therefore, the curves give evidence that with increasing concentration the internal segmental mobility is more and more suppressed. We interpret this as the consequence of the inhibited interpenetration. Therefore, an increase of the concentration much beyond the overlap concentration can be possible only if the samples become compressed, and this must inhibit the segmental mobility.

Conclusion

In this paper we studied turbid solutions of branched macromolecules with a tendency to aggregation. The main interest was to investigate the effects of multiple scattering in static and dynamic light scattering with such systems.

It is known that multiple scattering has a significant influence on the angular dependence of static light scattering for *globular colloid particles*. In dynamic light scattering multiple scattering leads to a faster decay of the time correlation function, resulting in too small values of the calculated hydrodynamic radii.

In general, the interpretation of light scattering experiments with macromolecules is more complicated because macromolecules are characterized by a fairly high segmental mobility that is missing in hard spheres. The segmental mobility is superimposed on the translational motion of the center of mass and contribute to the time correlation function. The question remained to which extent *multiple scattering* would modify time correlation functions *from turbid solutions of large macromolecules* with detectable segmental motion.

In static light scattering we found that the influence of multiple scattering on the angular dependence of the particle form factor for the branched amylopectin in water is surprisingly small. A closer inspection by means of Monte Carlo simulations revealed that the influence of multiple scattering decreases for a less pronounced angular dependence of the particle scattering factor. For the investigated macromolecules the angular dependence of the particle scattering factor is much weaker than for colloidal particles of the same radius. The reason for this behavior is based on the radial segment density that decreases in macromolecules when passing from the center toward the outskirts of the particle, whereas in hard spheres the segment density remains constant. This difference in the density distribution leads to a long tail toward large qR_g values. In other words, hard spheres have a fractal dimension of $d_f = 3$ while macromolecules are characterized by values of $d_f = 1.7-2.5$, depending on the extent of branching. Obviously, the lower the fractal dimension, the weaker the influence of multiple scattering is.

In any case a correction for the turbidity has to be applied if the absolute scattering intensity (Rayleigh ratio) is of interest. This correction yields, however, too high intensities, because in turbid systems only a fraction R^* of the scattering intensity originated from the coherent, singly scattered light. Only this coherent light with its defined phase correlations gives correct information on the shape and structure of the particles or macromolecules.

The influence of multiple scattering on the time dependence of correlation functions decreases when the particle diameters become large. The reason for this is that the value of the effective scattering vector of a multiple scattering system approaches that for a single scattering system when forward scattering becomes more pronounced. This is true at least in the detectable angular domain of light scattering ($\theta > 20°$).

The particle scattering factor of waxy maize starch varies more smoothly than for hard spheres; consequently, one would expect a more pronounced influence of multiple scattering for the macromolecules. But the waxy maize starch solution still shows strong forward scattering which can be roughly compared with that of hard spheres with $R_g = 115$ nm. It was shown experimentally[13] and by Monte Carlo simulations (Figure 3) that for such scattering characteristics the influence of multiple scattering on time correlation functions is hardly recognizable and often within the experimental limit.

The present paper gives an answer how multiple scattering affects the experimental data in static and dynamic light scattering in the case of macromolecules and how singly scattered light can be extracted. The effects on colloidal particles was already explored. A demanding task is still the investigation of *turbid gels*. The problem with these examples is even more complex because of the nonergodic behavior from inhomogeneities which have been found already in clear gels and whose motion appear largely frozen-in.

References and Notes

(1) Phillies, G. D. J. *Phys. Rev.* **1981**, *A24*, 1939.
(2) Schätzel, K. *J. Mod. Opt.* **1991**, *38*, 1849.
(3) Segré, P. N.; van Megen, W.; Pusey, P. N.; Schätzel, K.; Peters, W. *J. Mod. Opt.* **1995**, *42*, 1929.
(4) Aberle, L. B.; Wiegand, S.; Schröer, W.; Staude, W *Prog. Colloid Polym. Sci.* **1997**, *104*, 121.
(5) Overbeck, E.; Sinn, C.; Palberg, T.; Schätzel, K. *Colloids Surf., A* **1997**, *122*, 83.
(6) Meyer, W. V.; Cannell, D. S.; Smart, A. E.; Taylor, T. W.; Tin, P. *Appl. Opt.* **1997**, *36*, 7551.
(7) Nobbmann, U.; Jones, S. W.; Ackerson, B. J. *Appl. Opt.* **1997**, *26*, 77571.
(8) Aberle, L. B.; Schröer, W.; Staude, W. *Determination of particle size and differential scattering cross-section by 3D cross correlation technique*, XI. Conference of the European Colloid and Interface Society (ECIS 1997), Sept 14−19, 1997, Lunteren, The Netherlands.
(9) Aberle, L. B.; Hülstede, P.; Wiegand, S.; Schröer, W.; Staude, W. *Appl. Opt.* **1998**, *37*, 6511.
(10) (a) Urban, C.; Schurtenberger, P. *J. Colloid Interface Sci.* **1998**, *207*, 150, (b) *Prog. Colloid Polym. Sci.* **1998**, *110*, 61.
(11) Sinn, C.; Niehüser, R.; Overbeck, E.; Palberg, T. *Prog. Colloid Polym. Sci.* **1998**, *110*, 8.
(12) Aberle, L. B.; Kleemeier, M.; Hülstede, P.; Wiegand, S.; Schröer, W.; Staude, W. *Appl. Phys.* **1999**, *110*, 6511.
(13) Aberle, L. B.; Staude, W.; Hennemann, O.-D. *Phys. Chem. Chem. Phys.* **1999**, *1*, 3917.
(14) (a) Overbeck, E.; Sinn, C. *J. Mod. Opt.* **1999**, *46*, 202. (b) Overbeck, E.; Sinn, C.; Flammer, I.; Ricka, J. *Rev. Sci. Instrum.* **1998**, *69*, 3515. (c) Overbeck, E.; Sinn, C.; Palberg, J. *J. Mod. Opt.* **1999**, *46*, 303.
(15) Schröder, J.-M.; Wiegand, S. *Phys. Chem. Chem. Phys.* **2000**, *2*, 1493.
(16) Aberle, L. B.; Hülstede, P.; Kleemeier, M.; Staude, W.; Hennemann, O.-D. *Macromol. Symp.* **2000**, *162*, 249.
(17) Urban, C.; Romer, S.; Scheffold, F.; Schurtenberger, P. *Macromol. Symp.* **2000**, *162*, 235.
(18) Pusey, P. N. *Curr. Opin. Colloid Interface Sci.* **1999**, *4*, 177.
(19) Moussaid, A.; Pusey, P. N. *Phys. Rev. E* **1999**, *60*, 5670.
(20) Aberle, T.; Burchard, W.; Vorwerg, W.; Radosta, S. *Starch* **1994**, *46*, 329.
(21) The results depend to some extent on the preparation conditions. To obtain a molecularly disperse solution, the aqueous starch suspension has to be heated under argon atmosphere at 8 bar and 150 °C for 20 min. The reproducibility is affected with an estimated error of ±15% for M_w, ±12% for R_g, and ±6% for R_h.
(22) Burchard, W.; Schmidt, M.; Stockmayer, W. H. *Macromolecules* **1980**, *13*, 1265.
(23) Aberle, T.; Burchard, W. *Starch* **1997**, *49*, 215.
(24) (a) Schulz, L.; Burchard, W.; Dönges, R. In *Cellulose Derivatives, Modification, Characterization and Nanostructures*; Heinze, T. J., Glasser, W. G., Eds.; *ACS Symp. Ser.* **1998**, *688*, 218. (b) Schulz, L. Ph.D. Thesis, University of Freiburg, 1996. (c) Burchard, W. *Adv. Colloid Interface Sci.* **1996**, *64*, 45.
(25) Robin, J. P.; Mercier, Ch.; Duprat, F.; Carbonniere, R.; Guilbot, A. *Starch* **1975**, *7*, 36.

(26) Jenkins, P. J.; Cameron, R. E.; Donald, A. M.; Bras, W.; Derbyshire, G. E.; Mant, G. R.; Ryan, A. J. *J. Polym. Sci., Polym. Phys. Ed.* **1994**, *32*, 1579.
(27) Young, A. H. In *Starch, Chemistry and Technology*, 2nd ed.; Whistler, R. L., Bemiller, J. N., Paschall, E. F., Eds.; Academic Press: Orlando, FL, 1984; Chapter VIII.
(28) (a) Kohlrausch, R.; Poggendorff *Ann. Phys. Chem.* **1954**, *91*, 179; **1863**, *119*, 337. (b) Williams, G.; Watts, D. C. *Trans. Faraday Soc.* **1971**, *66*, 80. (c) Lindsey, C. P. Patterson, G. D. *J. Chem. Phys.* **1980**, *73*, 3348. (d) Patterson, G. D. *Adv. Polym. Sci.* **1983**, *48*, 148.
(29) Dubois-Violette. E.; de Gennes, P.-G. *Physics* **1967**, *3*, 181.
(30) Akcasu, A. Z.; Benmouna, M.; Han, C. C. *Polymer* **1980**, *21*, 866.
(31) Galinsky, G.; Burchard, W. *Macromolecules* **1997**, *30*, 6966.
(32) Trappe, V.; Bauer, J.; Weissmüller, M.; Burchard, W. *Macromolecules* **1997**, *30*, 2365.
(33) Cantow, H. J. *Makromol. Chem.* **1956**, *18/19*, 367.
(34) Ehl, J.; Loucheux, C.; Reiss, C.; Benoit, H. *Makromol. Chem.* **1964**, *75*, 35.
(35) Burchard, W. *Biomacromolecules* **2001**, *2*, 342.
(36) Bailey, A. E.; Cannell, D. S. *Phys. Rev. E* **1994**, *50*, 4853.

MA011202Y